Science Advances
AAAS

Supplementary Materials for

Mechanisms of sensory adaptation and inhibition of the cold and menthol receptor TRPM8

Ying Yin *et al.*

Corresponding author: Seok-Yong Lee, seok-yong.lee@duke.edu

Sci. Adv. **10**, eadp2211 (2024)
DOI: 10.1126/sciadv.adp2211

This PDF file includes:

Figs. S1 to S17
Table S1

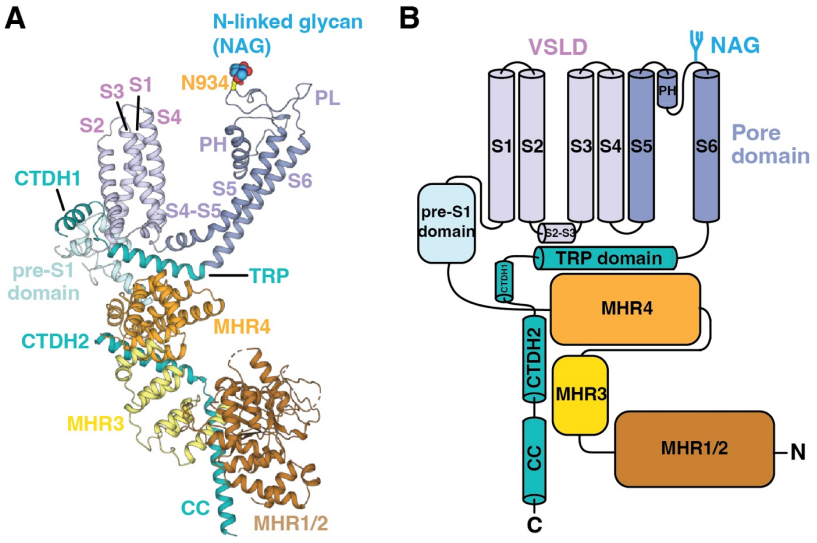

Fig. S1. Topology of TRPM8$_{MM}$ channels.

(**A** and **B**) Structural model (**A**) and cartoon diagram (**B**) delineating the topology of a single TRPM8$_{MM}$ protomer. The TRPM8$_{MM}$_AMTB structure from the current study was used for illustration, where the complete outer pore domain and an *N*-linked glycosylation moiety (NAG, blue) on the pore loop (PL) were resolved.

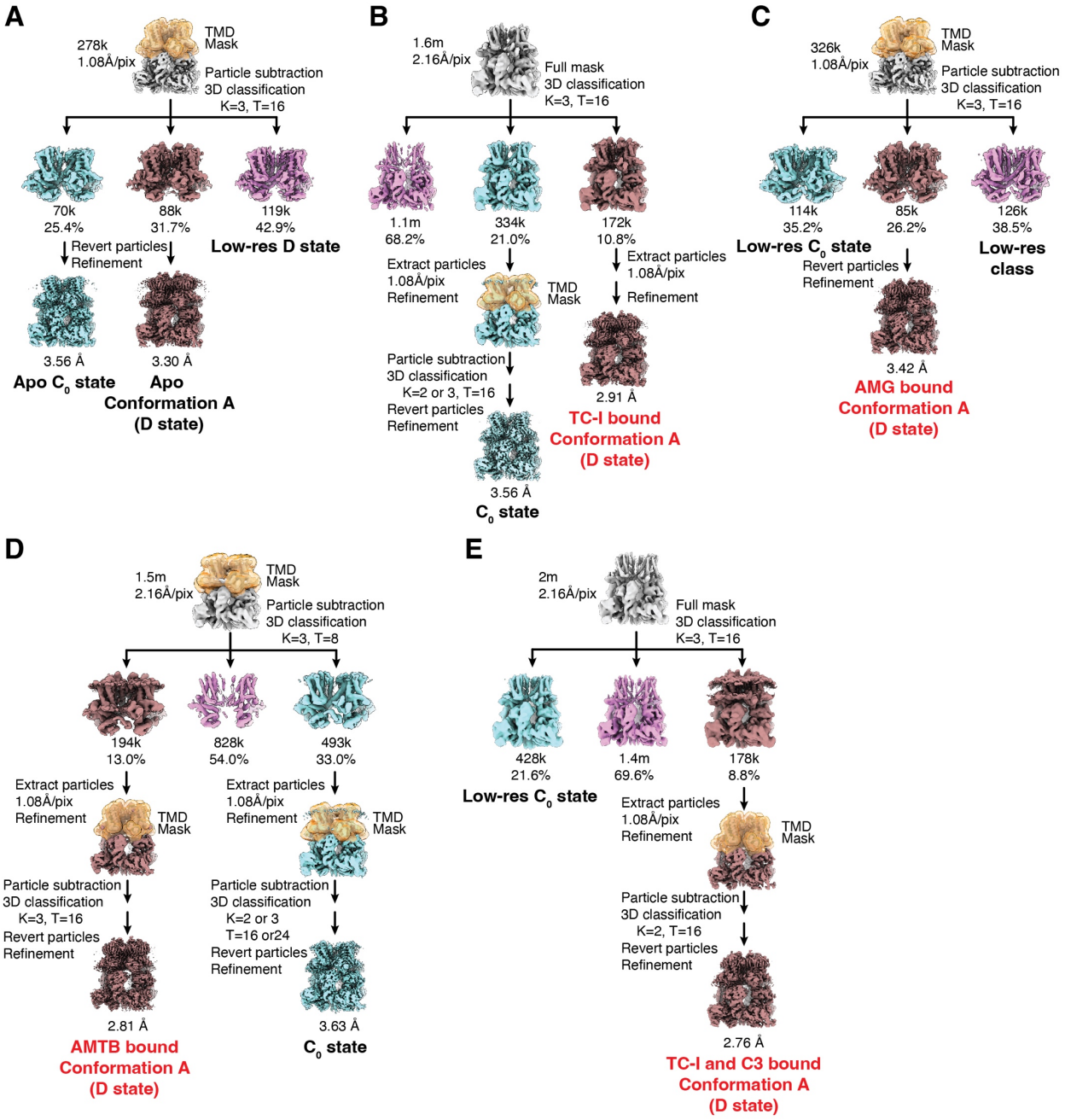

Fig. S2. Cryo-EM 3D classification of antagonists-bound TRPM8$_{MM}$ structures.

(**A**) TRPM8$_{MM}$ sample purified in LMNG and CHS in the absence of antagonists yielded 3D reconstructions in the distinct C_0 state and conformation A (D state).

(**B** to **E**) Cryo-EM 3D classification workflows to dissect the antagonist-bound conformation A reconstruction (D state) from the C_0-state reconstruction without antagonist bound and/or from the low-resolution reconstructions. Results are shown for TRPM8$_{MM}$ purified in LMNG and CHS and frozen in the presence of TC-I (**B**), AMG (**C**), AMTB (**D**), and TC-I plus C3 (**E**). TMD masks used for particle subtraction and 3D classification jobs in RELION are shown in transparent orange color.

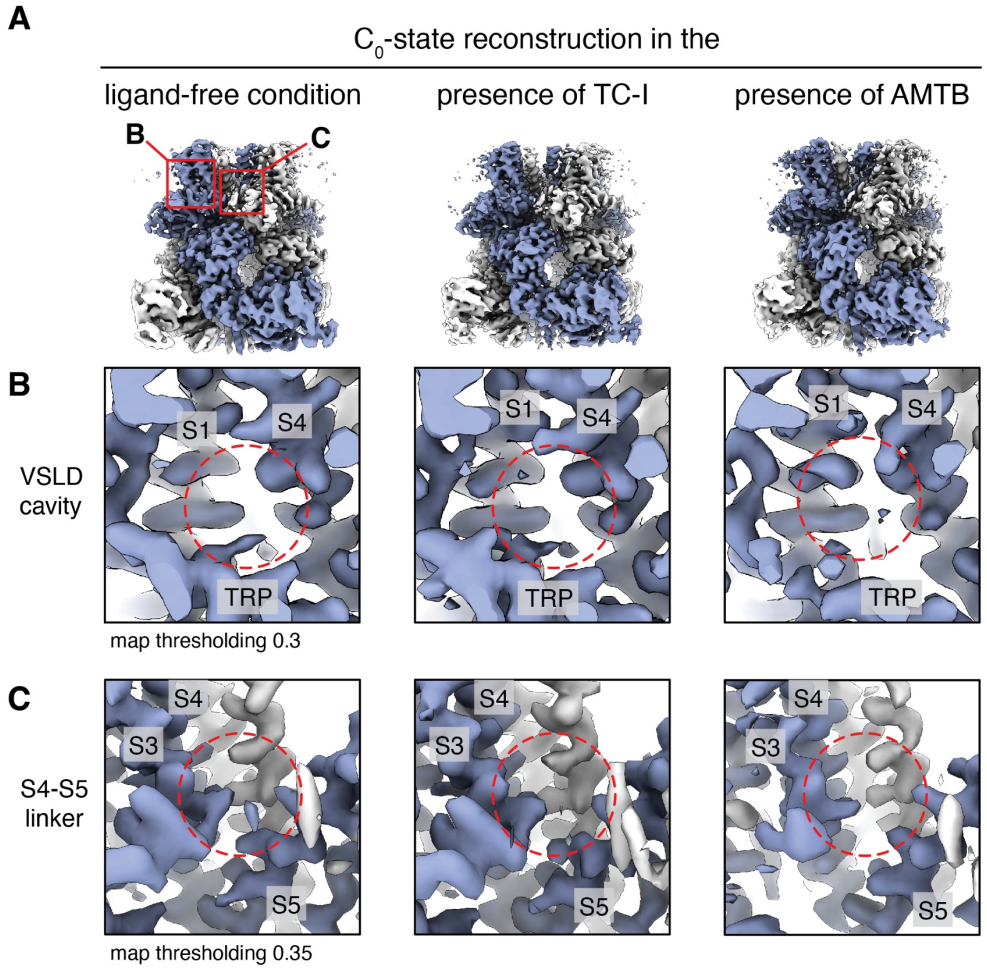

Fig. S3. The absence of strong EM density for antagonists in the C_0-state 3D reconstructions.

(**A**) 3D reconstructions in the C_0-state conformation resolved from cryo-EM datasets prepared in the ligand-free condition (left), in the presence of TC-I (center) and AMTB (right). Thresholding 0.2, 0.23, 0.19.

(**B** and **C**) Close-up views at the VSLD cavity (**B**) and the S4-S5 linker (**C**) from (**A**). Red dashed circles highlight the absence of strong and unambiguous EM densities for antagonists at the corresponding locations. Thresholding 0.3 in (**B**) and 0.35 in (**C**).

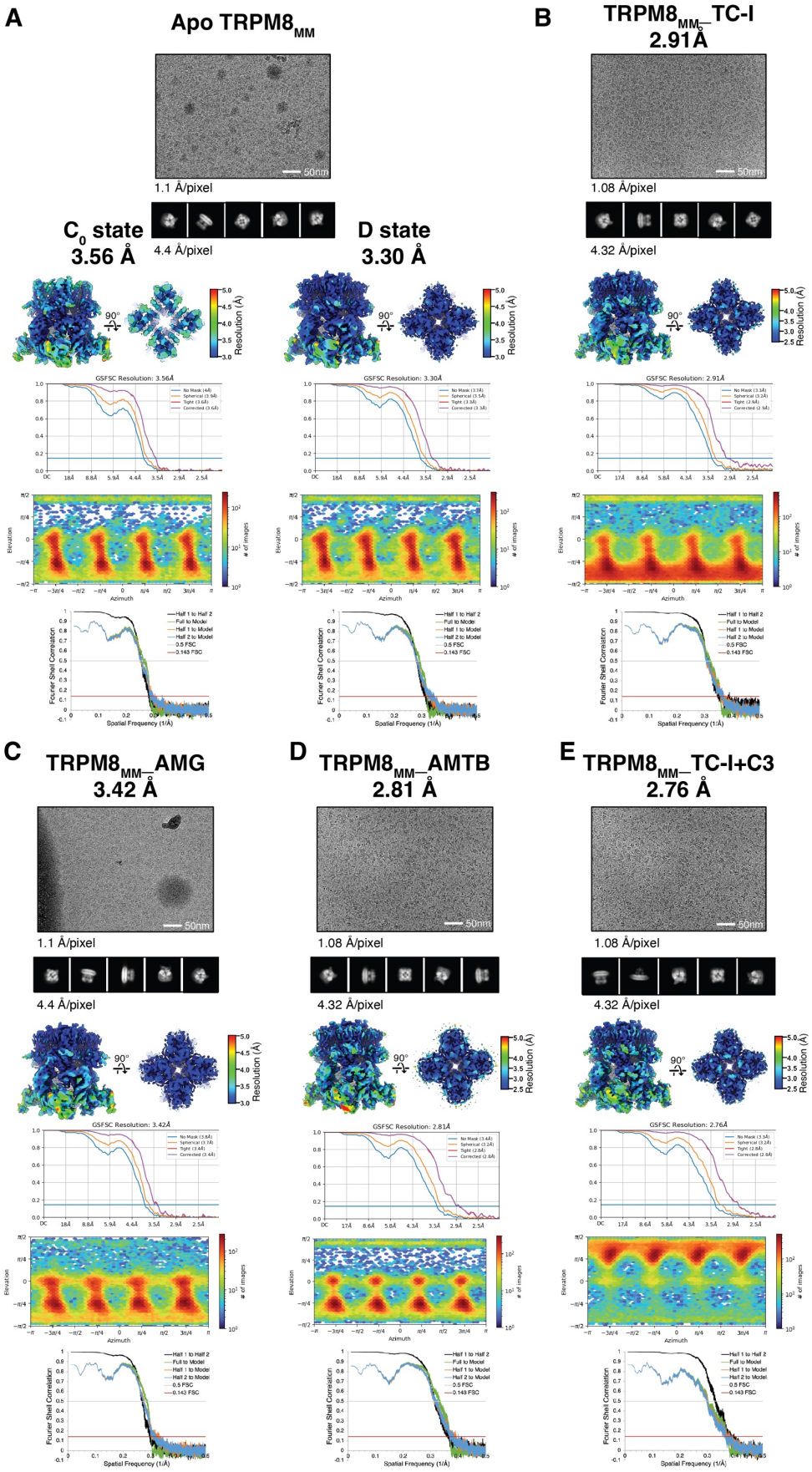
A
Apo TRPM8MM
1.1 Å/pixel
4.4 Å/pixel
C0 state
3.56 Å
D state
3.30 Å
B
TRPM8MM–TC-I
2.91 Å
1.08 Å/pixel
4.32 Å/pixel
C
TRPM8MM–AMG
3.42 Å
1.1 Å/pixel
4.4 Å/pixel
D
TRPM8MM–AMTB
2.81 Å
1.08 Å/pixel
4.32 Å/pixel
E
TRPM8MM–TC-I+C3
2.76 Å
1.08 Å/pixel
4.32 Å/pixel
50nm
90°
Resolution (Å)
GSFSC Resolution: 3.56Å
GSFSC Resolution: 3.30Å
GSFSC Resolution: 2.91Å
GSFSC Resolution: 3.42Å
GSFSC Resolution: 2.81Å
GSFSC Resolution: 2.76Å
Elevation
Azimuth
# of images
Fourier Shell Correlation
Spatial Frequency (1/Å)
Half 1 to Half 2
Full to Model
Half 1 to Model
Half 2 to Model
0.5 FSC
0.143 FSC

Fig. S4. Cryo-EM data collection and validation, part I.

(**A** to **E**) Representative micrographs, 2D classification images, local resolution estimation, the Fourier shell correlation (FSC) curves of the final 3D reconstruction with different masking calculated in CryoSPARC, orientation distribution diagram, and the FSC curves between model and full- or half-maps calculated in PHENIX. Results are shown for cryo-EM datasets of $TRPM8_{MM}$ prepared in the absence of antagonists or agonists (**A**), and in the presence of TC-I (**B**), AMG (**C**), AMTB (**D**), and TC-I plus C3 (**E**), respectively. The pixel sizes of micrographs and 2D class averages are specified below the image.

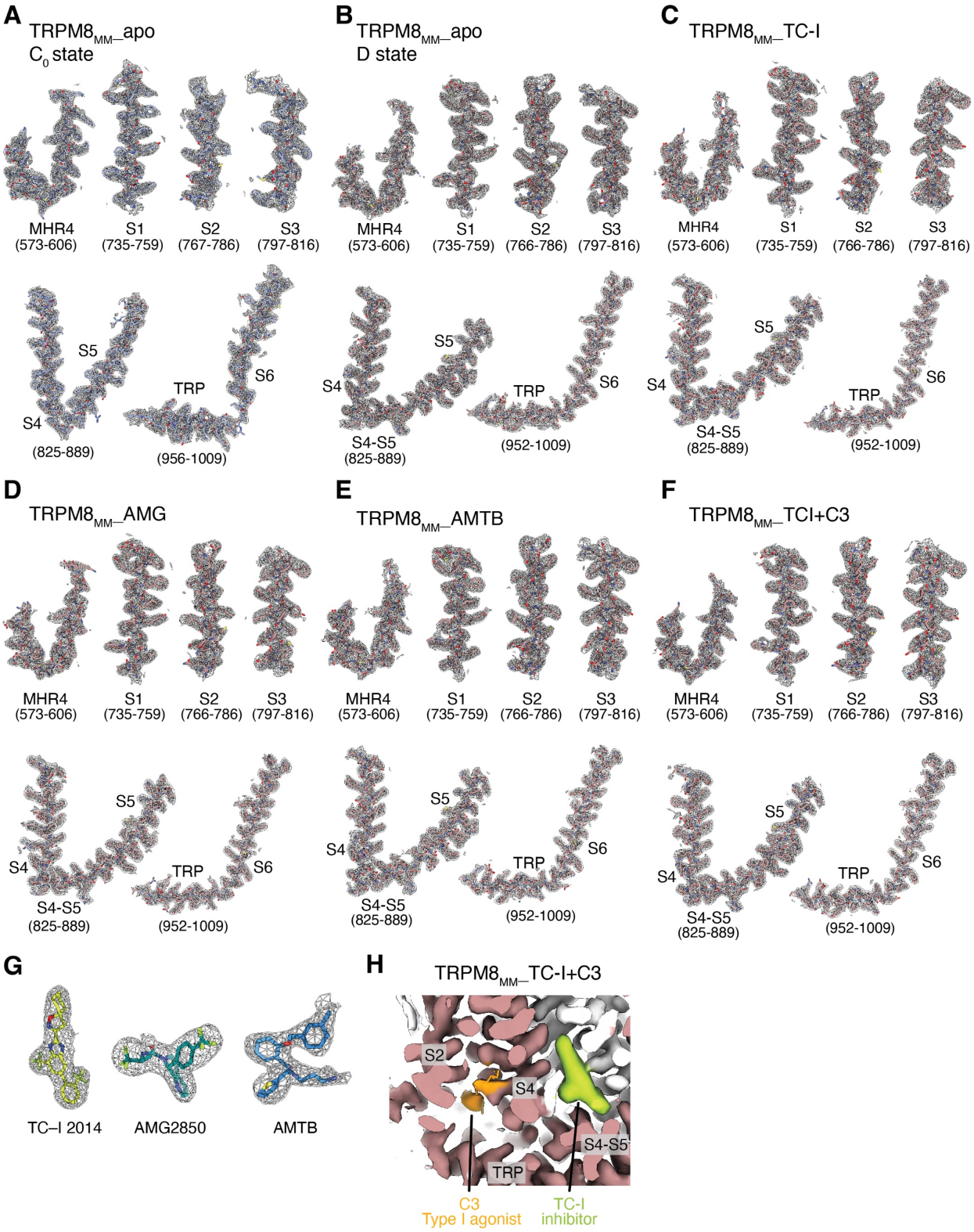

Fig. S5. Cryo-EM density quality for the TRPM8$_{MM}$ structures.

(**A** to **F**) Representative EM densities (gray mesh) for key structural elements in C_0-state TRPM8$_{MM}$_apo (**A**), D-state TRPM8$_{MM}$_apo (**B**), TRPM8$_{MM}$_TC-I (**C**), TRPM8$_{MM}$_AMG (**D**), TRPM8$_{MM}$_AMTB (**E**), and TRPM8$_{MM}$_TC-I+C3 (**F**). Thresholding 0.14 or 0.2 in (**A**), 0.2 in (**B** to **F**). Residue ranges are indicated.

(**G**) EM densities (gray mesh) for antagonists TC-I, AMG, and AMTB. Thresholding 0.2.

(**H**) Close-up view depicting EM densities for C3 (orange) in the VSLD cavity and for TC-I (lime) at the S4-S5 linker in the $TRPM8_{MM}$_TC-I+C3 reconstruction. Neighboring protomers colored in brown and gray. Thresholding 0.22. Residue sidechains and antagonists are shown as sticks in (**A** to **G**).

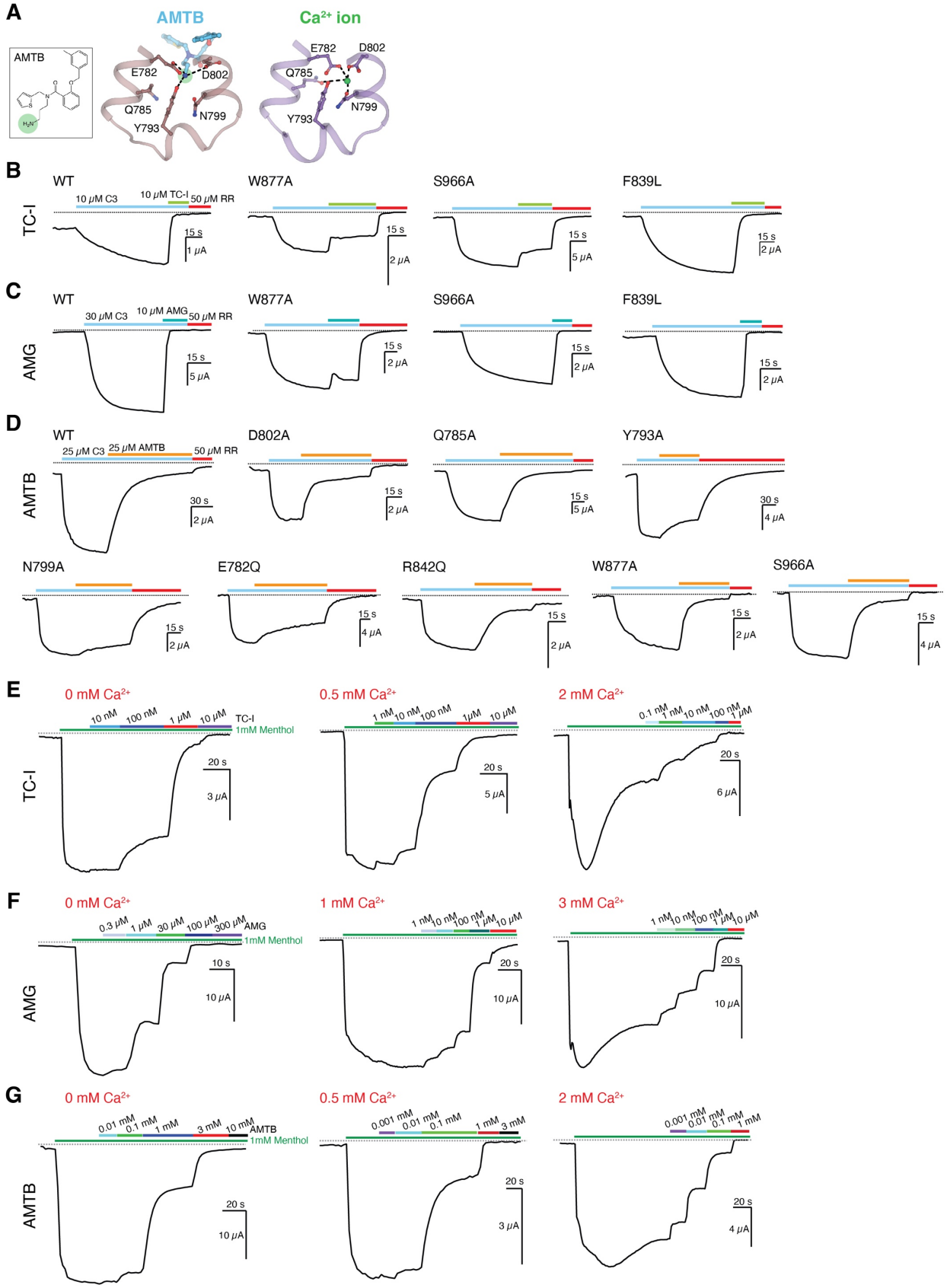

Fig. S6. Functional characterizations of antagonists on TRPM8MM channels.

(**A**) Comparison between the AMTB amine group interaction (left) and the Ca^{2+} ion coordination (right, PDB 8E4L) in the VSLD cavity.

(**B** to **D**) Representative TEVC recordings on the WT and mutant $TRPM8_{MM}$ channels at –60mV. Horizontal colored lines represent the application of C3 (blue), TC-I (**B**, lime), AMG (**C**, teal), AMTB (**D**, orange), and ruthenium red (RR) as indicated.

(**E** to **G**) Representative TEVC recordings of WT $TRPM8_{MM}$ at –60 mV. Horizontal colored lines indicated applications of 1 mM menthol followed by increasing concentrations of TC-I (**E**), AMG **(F**), and AMTB (**G**) in the presence of zero (left panels), low (middle panels), and high (right panels) concentrations of extracellular Ca^{2+} as indicated in the figures.

Dotted lines in **B** to **G** indicate the zero-current level.

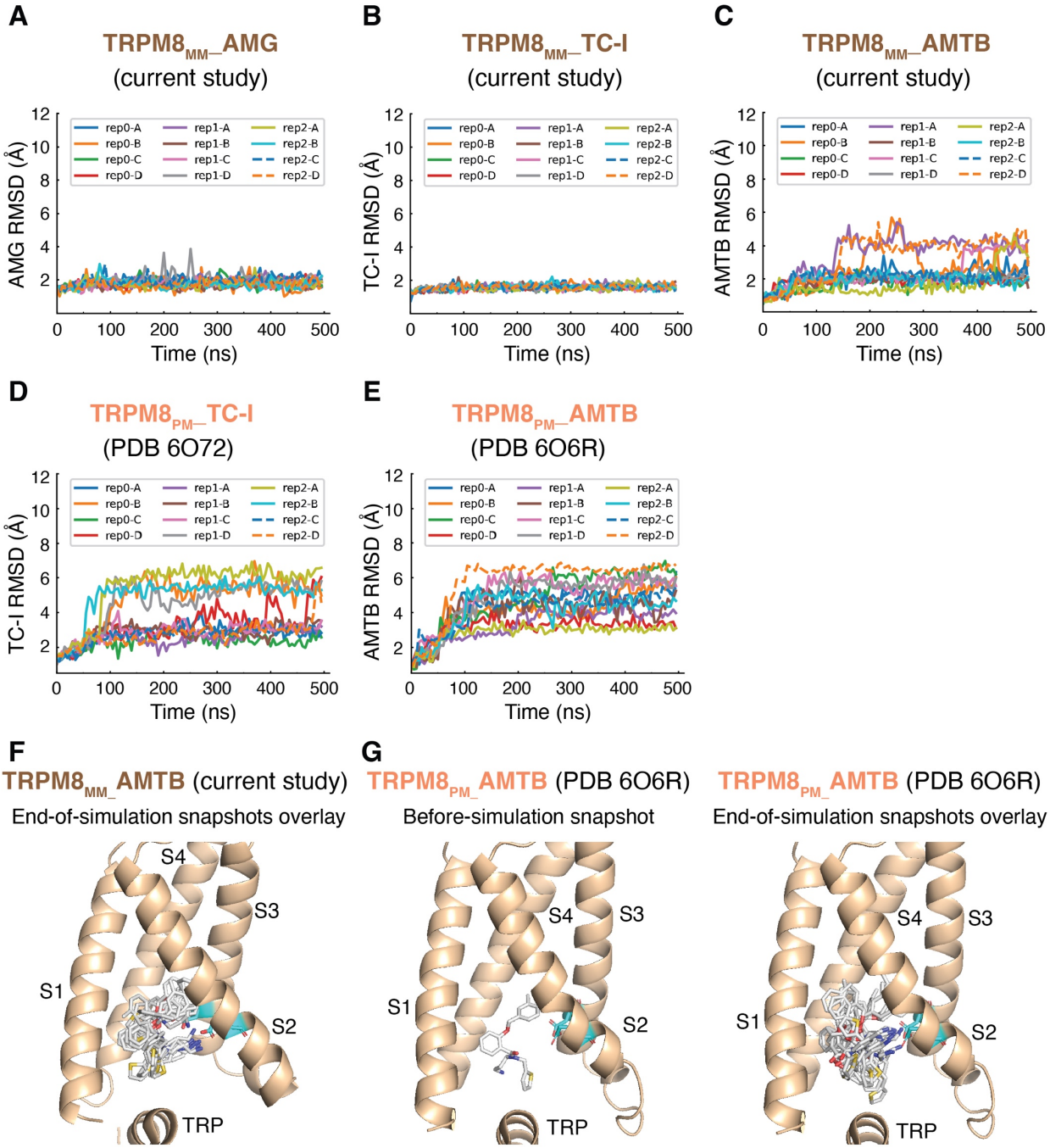

Fig. S7. Molecular dynamics (MD) simulations of antagonist binding to TRPM8$_{MM}$ and TRPM8$_{PM}$ channels.

(**A** to **C**) Ligand RMSD of AMG (**A**), TC-I (**B**), and AMTB (**C**) in the TRPM8$_{MM}$ structures from the current study, during the simulation time course of each replicate (3 replicas for each assembly) with an averaged RMSD of 1.6 Å for TC-I, 1.8 Å for AMG, and 2.5 Å for AMTB, calculated from the last 200-ns trajectories.

(**D** and **E**) Ligand RMSD of TC-I (**D**; PDB 6O72) and AMTB (**E**; PDB 6O6R) in the published TRPM8$_{PM}$ structures, during the simulation time course of each replicate (3 replicas for each assembly), with an averaged RMSD of 3.7Å for TC-I and 4.9 Å for AMTB, calculated from the last 200-ns trajectories.

(**F**) Overlay of the end-of-simulation snapshots of AMTB in the TRPM8$_{MM}$_AMTB structure from the current study.

(**G**) Comparison of the before-simulation snapshot (left) and the overlaid end-of-simulation snapshots (right) of AMTB in the published TRPM8$_{PM}$_AMTB structure (PDB 6O6R). AMTB shown as sticks in (**F**) and (**G**).

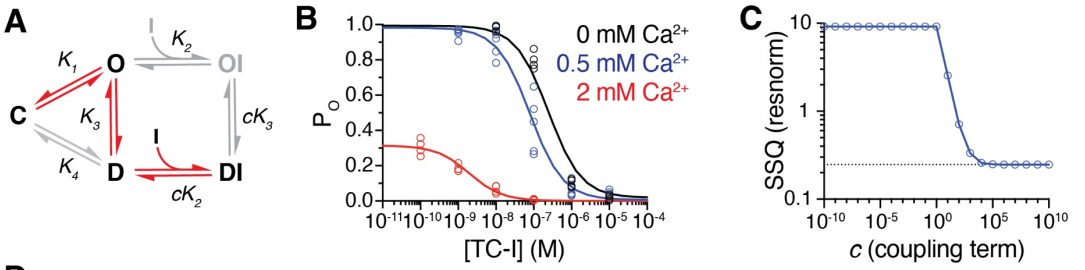

D

Model Parameter	AMG	TC-I
K_1	≥10^3 (fixed at 10^3)	≥10^3 (fixed at 10^3)
K_2 (M^{-1})	7.5×10^3 [3.8×10^3 – 11.2×10^3]	7.5×10^4 [0.13×10^4 – 13×10^4]
K_3 no Ca^{2+}	0.011 [0.0051 – 0.016]	0.0054 [0.00099 – 0.0098]
K_3 low Ca^{2+}	0.058 [0.031 – 0.085]	0.017 [0.0032 – 0.031]
K_3 high Ca^{2+}	0.57 [0.45 – 0.69]	2.18 [1.7 – 2.6]
c (coupling)	≥10^4 (fixed at 10^4)	≥10^4 (fixed at 10^4)

	Open State ($1/K_2$)	Desensitized State ($1/cK_2$)
K_D (AMG)	130 ± 33 μM	13 ± 3 nM
K_D (TC-I)	13 ± 6 μM	1.3 ± 0.6 nM

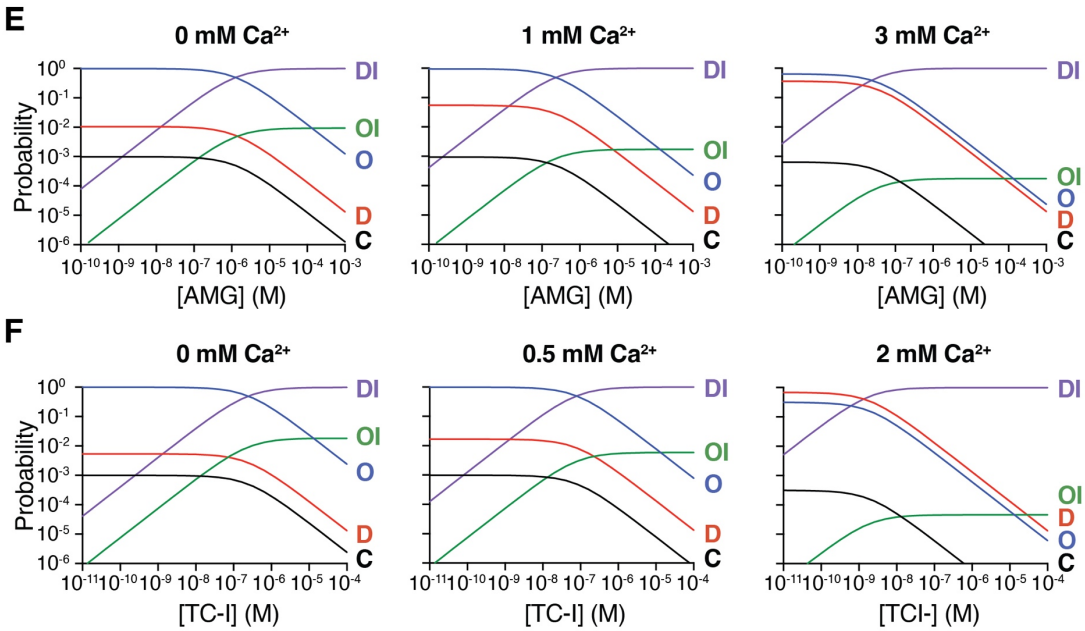

Fig. S8. Thermodynamic modeling.

(**A**) Thermodynamic model of TRPM8 desensitization and inhibitor binding for the equilibria (K_n) among closed (C), open (O), desensitized (D), and inhibitor-bound (OI, DI) states and associated thermodynamic coupling (c). The red arrows indicate transition among the thermodynamically favored states, based on fit values.

(**B**) TC-I dose-response data fit with the thermodynamic model for 0 mM, 0.5 mM, and 2 mM extracellular Ca^{2+}. Data comes from **Fig. 2A**, taking into account the initial level of desensitization. Datapoints for individual replicate ($n \geq 4$) shown.

(**C**) Model fit quality as sum of squared residuals (SSQ or resnorm) plotted as a function of fixed coupling parameter (c) value.

(**D**) Model fitting parameters and [95% confidence intervals] for AMG and TC-I data. Calculated K_D values for inhibitor to O and D states with errors propagated from parameter confidence intervals.

(**E**) Species populations as a function of AMG concentration based on model fitting parameters in (**D**). Closed (black), open (blue), desensitized (red), inhibitor-bound open (green), and inhibitor-bound desensitized (purple).

(**F**) Species populations as a function of TC-I concentration based on model fitting parameters in (**D**) and colored as in (**E**).

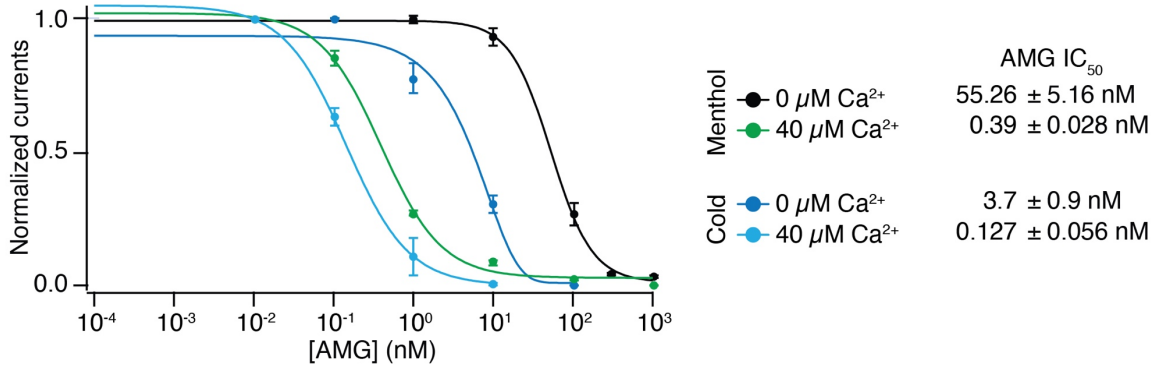

Fig. S9. Concentration-response relationships for AMG in inhibiting TRPM8$_{MM}$ activation by different stimuli.

Normalized concentration-response relations for AMG against the WT TRPM8$_{MM}$ activation by cold or menthol in the presence of 0 μM and 40 μM extracellular Ca^{2+} (n = 3–4), respectively. Data are mean ± SEM. The continuous curves were fit to the Hill equation with IC_{50} values indicated in the figure.

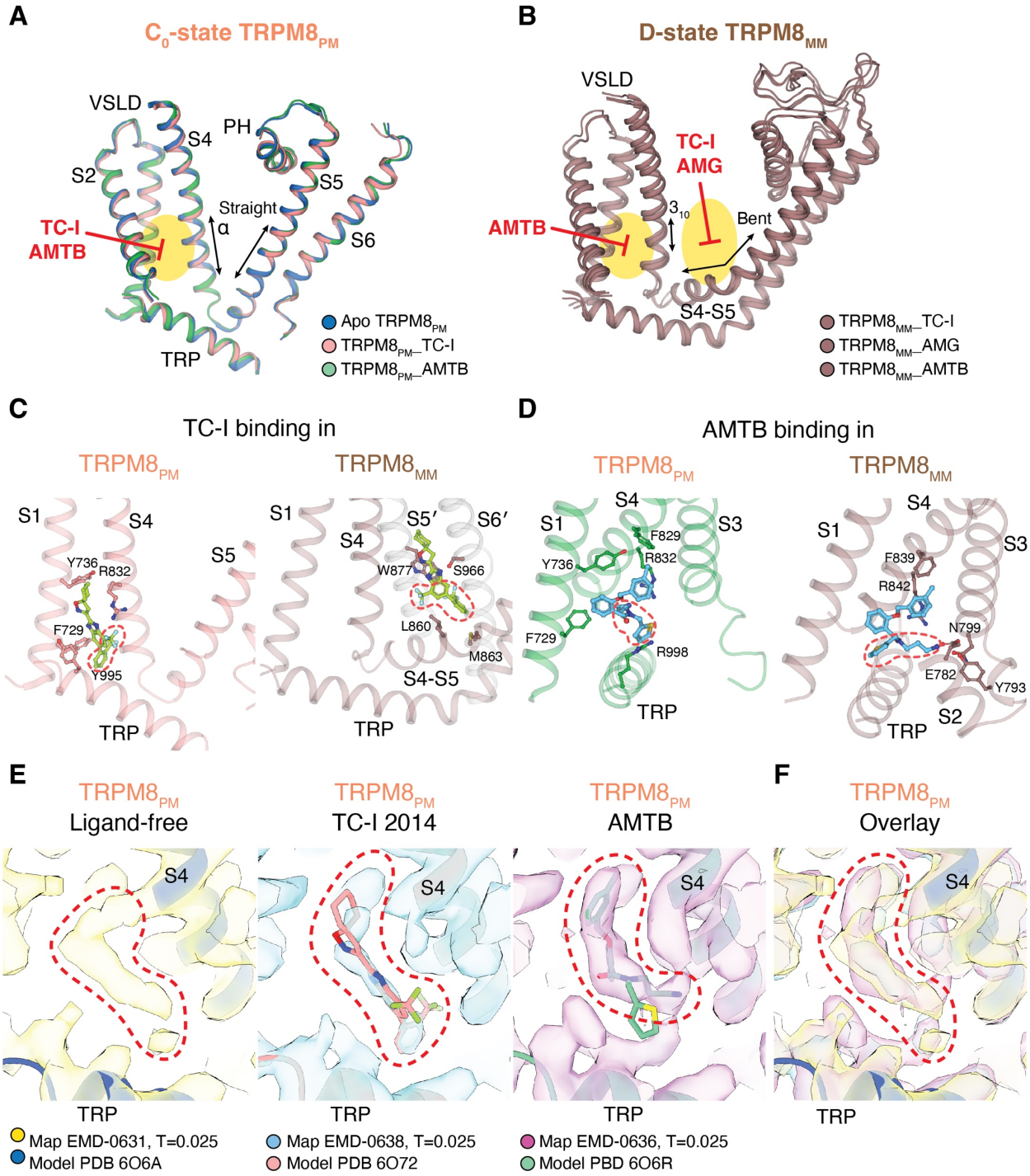

Fig. S10. Comparison of inhibitor binding in TRPM8PM and TRPM8MM structures.

(**A**) Published TRPM8PM structures determined in the ligand-free (apo) and in the presence of TC-I and AMTB, respectively, adopt the C_0-state conformation. TC-I and AMTB molecules were modeled to bind in the VSLD cavity, as indicated by the yellow shades and red arrows.

(**B**) TRPM8MM structures from the current study determined in the presence of TC-I, AMG, and AMTB, respectively, adopt the D-state conformation. TC-I and AMG bind above the S4-S5 linker and AMTB binds in the VSLD cavity, as indicated by the yellow shades and red arrows.

(**C**) Comparison of TC-I binding in the published $TRPM8_{PM}$ structure (left) and in $TRPM8_{MM}$ (right). Red dotted circles highlight the different binding poses.

(**D**) Comparison of AMTB binding in the published $TRPM8_{PM}$ structure (left) and in $TRPM8_{MM}$ (right). Red dotted circles highlight the different binding poses.

(**E**) Superimposition of the PDB model and cryo-EM map for the published $TRPM8_{PM}$ structures determined in the ligand-free condition and in the presence of TC-I and AMTB, respectively. Similarly shaped EM density peaks (red dotted lines) are present in the VSLD cavity of all three maps.

(**F**) Superimposition of the three cryo-EM maps from (**E**) with the ligand-free $TRPM8_{PM}$ structure, showing similarly shaped EM density peaks (red dotted lines) are present in the VSLD cavity in all three maps.

EMD IDs for cryo-EM maps and PDB IDs for structural models that were previously reported for $TRPM8_{PM}$ are indicated in the figure. Key residues and modeled antagonists shown as sticks. Cryo-EM maps shown as colored transparent surface in (**E**) and (**F**).

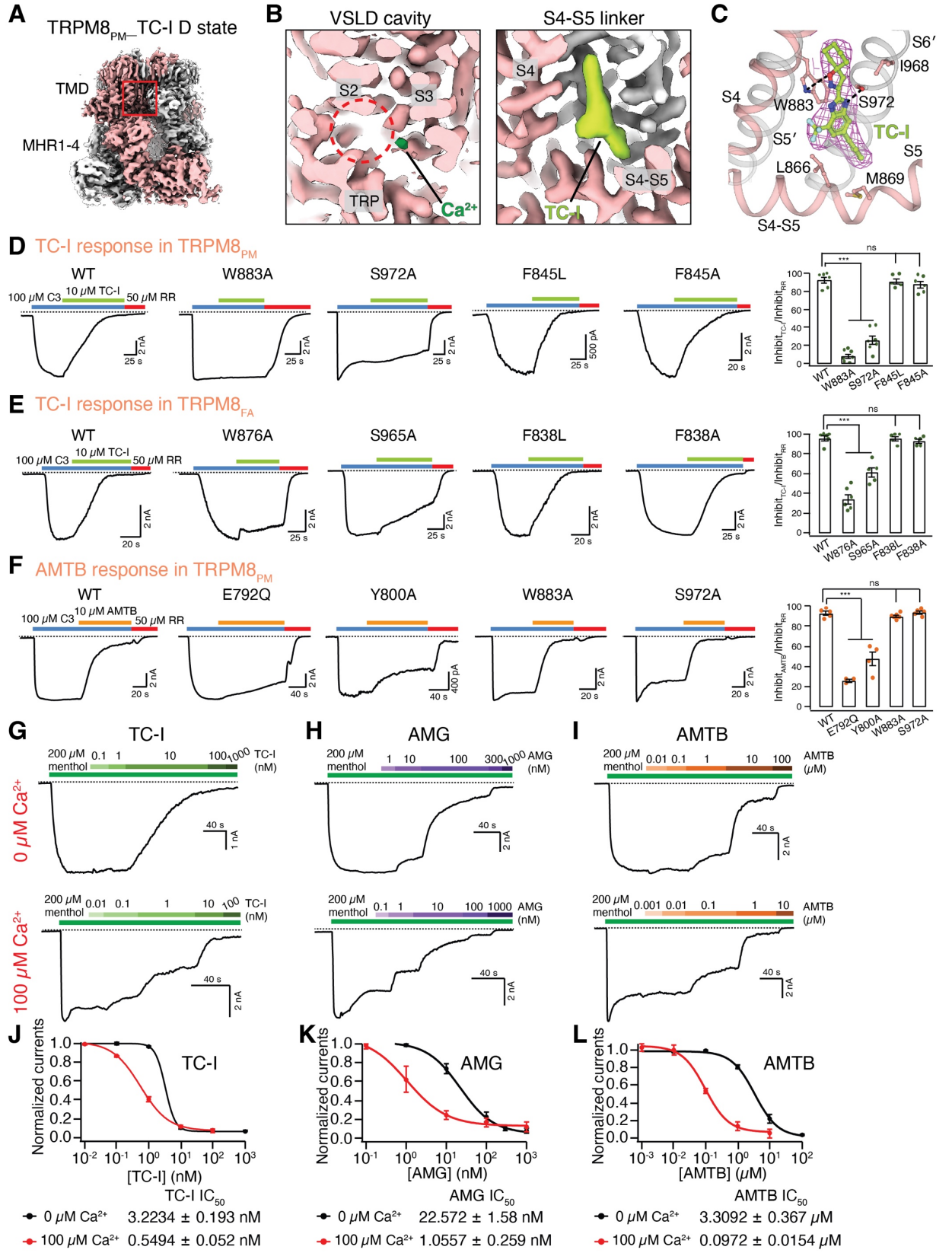

Fig. S11. Structural and functional validation of antagonist binding in the avian TRPM8$_{PM}$ channel from the current study.

(**A**) 3D reconstruction of $TRPM8_{PM}$ in complex with TC-I and Ca^{2+} in the D state conformation. Neighboring protomers are colored in light pink and gray, respectively. Thresholding 0.25.

(**B**) Close-up views of the EM density at the VSLD cavity (left) and the S4-S5 linker (right) from the reconstruction in (**A**). Red dashed circle indicates the lack of TC-I density in the VSLD cavity. Densities for Ca^{2+} and TC-I colored in green and lime, respectively. Thresholding 0.25 in the left panel and 0.6 in the right panel.

(**C**) The binding site and EM density for TC-I (lime sticks). Densities (magenta mesh) contoured at thresholding 0.26 for TC-I. Neighboring protomers colored in pink and gray, respectively.

(D) Representative currents of the WT and mutant $TRPM8_{PM}$ channels at –60 mV in HEK293T cells. Horizontal colored lines represent the application of 100 μM C3 (blue), 10 μM TC-I (lime), and ruthenium red (RR) as indicated. Summary of current inhibition by 10 μM TC-I in HEK293T cells expressing WT and mutant $TRPM8_{PM}$ channels (n = 5–7). Dots indicate the individual data points for each experiment. ns > 0.05, ***P < 0.001, using one-way ANOVA followed by Dunnett post-hoc test. Data are mean ± SEM.

(E) Representative currents of the WT and mutant flycatcher TRPM8 ($TRPM8_{FA}$) channels at –60 mV in HEK293T cells. Horizontal colored lines represent the application of 100 μM C3 (blue), 10 μM TC-I (lime), and RR as indicated. Summary of current inhibition by 10 μM TC-I in HEK293T cells expressing WT and mutant $TRPM8_{FA}$ channels (n = 5–6). Dots indicate the individual data points for each experiment. ns > 0.05, ***P < 0.001, using one-way ANOVA followed by Dunnett post-hoc test. Data are mean ± SEM.

(F) Representative currents of the WT and mutant $TRPM8_{PM}$ channels at –60 mV in HEK293T cells. Horizontal colored lines represent the application of 100 μM C3 (blue), 10 μM AMTB (orange), and RR as indicated. Summary of current inhibition by 10 μM AMTB in HEK293T cells expressing WT and mutant $TRPM8_{PM}$ channels (n = 3–6). Dots indicate the individual data points for each experiment. ns > 0.05, ***P < 0.001, using one-way ANOVA followed by Dunnett post-hoc test. Data are mean ± SEM.

(**G** to **I**) Representative current traces of the WT $TRPM8_{PM}$ channels at –60 mV in HEK293T cells. Current trace elicited by 200 μM menthol was inhibited by increasing concentrations of TC-I (**G**), AMG (**H**), and AMTB (**I**) in the presence of 0 μM (top) or 100 μM (bottom) extracellular Ca^{2+}.

(**J** to **L**) Normalized concentration-response relations for TC-I (**J**), AMG (**K**), and AMTB (**L**) against the WT $TRPM8_{PM}$ activation by 200 μM menthol in the presence of 0 μM (black trace, n = 4–5) or 100 μM (red trace, n = 4) extracellular Ca^{2+}. Data are mean ± SEM. The continuous curves were fit to the Hill equation with IC_{50} values indicated in the figure.

Dotted lines in **D** to **I** indicate the zero-current level.

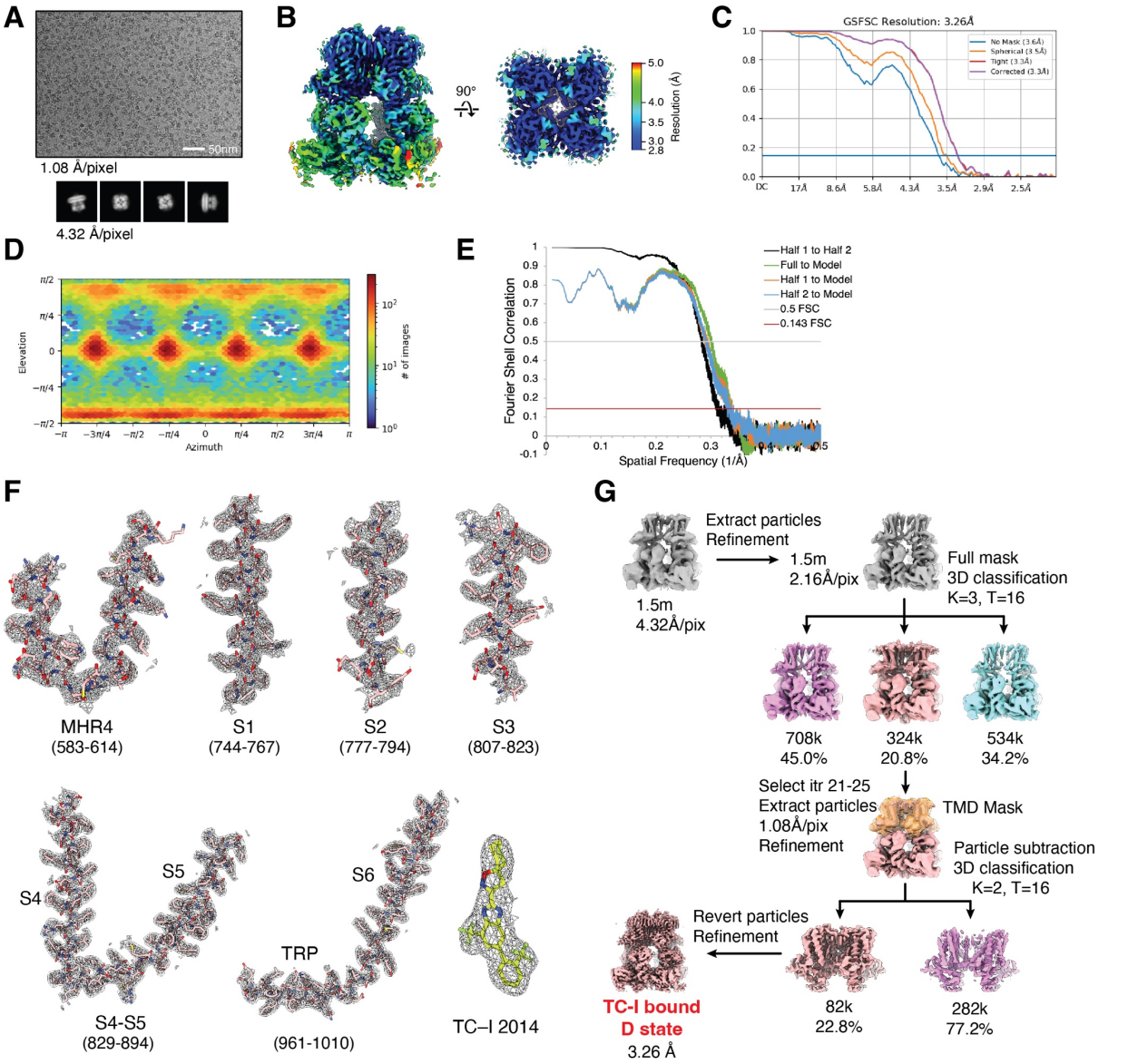

Fig. S12. Cryo-EM data processing and validation, part II, for the TRPM8$_{PM}$_TC-I structure in the current study.

(**A**) Representative micrographs and 2D classification images. The pixel sizes are specified below the images.

(**B**) Local resolution estimation.

(**C**) The Fourier shell correlation (FSC) curves of the final 3D reconstruction with different masking calculated in CryoSPARC,

(**D**) Orientation distribution diagram.

(**E**) the FSC curves between model and full- or half-maps calculated in PHENIX.

(**F**) Representative EM densities (gray mesh) for key structural elements and TC-I. Thresholding 0.25.

(**G**) Cryo-EM 3D classification workflow to dissect the TC-I bound reconstruction for the TRPM8$_{PM}$ channel. TMD mask used for particle subtraction and 3D classification jobs in RELION shown in transparent orange color.

```
                                                                S1
Human_TRPM8          CLFIIPLVGCGFVSFRKKPVDKHKKLLWYYVAFFTSPFVVFSWNVVFYIAFLLLFAYVLL     757
Mouse_TRPM8          CLFIIPLVGCGLVSFRKKPIDKHKKLLWYYVAFFTSPFVVFSWNVVFYIAFLLLFAYVLL     757
Rat_TRPM8            CLFIIPLVGCGLVSFRKKPIDKHKKLLWYYVAFFTSPFVVFSWNVVFYIAFLLLFAYVLL     757
Chicken_TRPM8        CLFFFPLIGCGFISFRKKPVEKSKKLFLYYVSFFTSPFVVFSWNVIFYIVFLLLFAYVLL     757
Flycatcher_TRPM8     CLFFFPLIGCGFISFRKKPVEKTKKLFLYYVSFFTSPFVVFSWNVIFYIAFLLLFAYVLL     780
Great_tit_TRPM8      CLFFFPLIGCGFISFRKKPVEKSKKLFLYYVSFFTSPFVVFSWNVIFYIAFLLLFAYVLL     767
                     ***::**:***::******::* ***: ***:**************:***.**********

                                S2                  S2-S3          S3
Human_TRPM8          MDFHSVPHPPELVLYSLVFVLFCDEVRQWYVNGVNYFTDLWNVMDTLGLFYFIAGIVFRL     817
Mouse_TRPM8          MDFHSVPHTPELILYALVFVLFCDEVRQWYMNGVNYFTDLWNVMDTLGLFYFIAGIVFRL     817
Rat_TRPM8            MDFHSVPHTPELILYALVFVLFCDEVRQWYMNGVNYFTDLWNVMDTLGLFYFIAGIVFRL     817
Chicken_TRPM8        MDFQKEPTVLEIILYVLVFILLCDEVRQWYMNGSKYLSDLWNVMDTLAIFYFIAGIVLRL     817
Flycatcher_TRPM8     MDFQKEPTALEIILYVLVFILLCDEVRQWYMNGSKYFSDLWNVMDTLAIFYFIAGIVFRL     840
Great_tit_TRPM8      MDFQKEPTALEIILYVLVFVLLCDE---WYMNGSKYFSDLWNVMDTLAIFYFIAGIVFRL     824
                     ***:. *   *::** ***:*:***   **:** :*::*********.:********:**

                          S4                      S4-S5          S5
Human_TRPM8          HSSNKSSLYSGRVIFCLDYIIFTLRLIHIFTVSRNLGPKIIMLQRMLIDVFFFLFLFAVW     877
Mouse_TRPM8          HSSNKSSLYSGRVIFCLDYIIFTLRLIHIFTVSRNLGPKIIMLQRMLIDVFFFLFLFAVW     877
Rat_TRPM8            HSSNKSSLYSGRVIFCLDYIIFTLRLIHIFTVSRNLGPKIIMLQRMLIDVFFFLFLFAVW     877
Chicken_TRPM8        HSSNESSWYSGRVIFCLDYIVFTLRLIHIFTVSRNLGPKIIMLQRMMIDVFFFLFLFAVW     877
Flycatcher_TRPM8     HS-DESSWYSGRVIFCLDYIVFTLRLIHIFTVSRNLGPKIIMLQRMMIDVFFFLFLFAVW     899
Great_tit_TRPM8      HS-DESSWYSGRVIFCLDYIVFTLRLIHIFTVSRNLGPKIIMLQRMMIDVFFFLFLFAVW     883
                     ** ::** ************:************************:*************

                     S5          PH
Human_TRPM8          MVAFGVARQGILRQNEQRWRWIFRSVIYEPYLAMFGQVPSDVDGTTYDFAHCTFTGNESK     937
Mouse_TRPM8          MVAFGVARQGILRQNEQRWRWIFRSVIYEPYLAMFGQVPSDVDSTTYDFSHCTFSGNESK     937
Rat_TRPM8            MVAFGVARQGILRQNEQRWRWIFRSVIYEPYLAMFGQVPSDVDSTTYDFSHCTFSGNESK     937
Chicken_TRPM8        MVAFGVARQGILRKNEHRWEWIFRSVIYEPYLAMFGQYPDDVDGTTYNFDRCTFSGNESK     937
Flycatcher_TRPM8     MVAFGVARQGILRKNEHRWEWIFRSVIYEPYLAMFGQYPDDIDGTTYNFDHCTFSGNESK     959
Great_tit_TRPM8      MVAFGVARQGILRKNEHRWEWIFRSVIYEPYLAMFGQYPDDIDGTTYNFDRCTFSGNESK     943
                     **************:**:**.***************** *.*:*.***:* :***:*****

                                   S6                          TRP
Human_TRPM8          PLCVELDEHNLPRFPEWITIPLVCIYMLSTNILLVNLLVAMFGYTVGTVQENNDQVWKFQ     997
Mouse_TRPM8          PLCVELDEHNLPRFPEWITIPLVCIYMLSTNILLVNLLVAMFGYTVGIVQENNDQVWKFQ     997
Rat_TRPM8            PLCVELDEYNLPRFPEWITIPLVCIYMLSTNILLVNLLVAMFGYTVGIVQENNDQVWKFQ     997
Chicken_TRPM8        PLCVELDANNQPRFPEWITIPLVCIYMLSTNILLVNLLVAMFGYTVGSVQENNDQVWKFQ     997
Flycatcher_TRPM8     PLCVELDANNQPRFPEWITIPLVCIYMLSTNILLVNLLVAMFGYTVGSVQENNDQVWKFQ     1019
Great_tit_TRPM8      PLCVELDANNQPRFPEWITIPLVCIYMLSTNILLVNLLVAMFGYTVGSVQENNDQVWKFQ     1003
                     *******  * ************************************ ************

                     TRP
Human_TRPM8          RYFLVQEYCSRLNIPFPFIVFAYFYMVVKKCFKCCCKEKNMESSVCCFKNEDNETLAWEG     1057
Mouse_TRPM8          RYFLVQEYCNRLNIPFPFVVFAYFYMVVKKCFKCCCKEKNMESNACCFRNEDNETLAWEG     1057
Rat_TRPM8            RYFLVQEYCNRLNIPFPFVVFAYFYMVVKKCFKCCCKEKNTESSACCFRNEDNETLAWEG     1057
Chicken_TRPM8        RYFLVQEYCSRLTIPFPFVIFAYIFMVMRKCFKCCCKNESKEPSICCSRNEDNETLSWEA     1057
Flycatcher_TRPM8     RFFLVQEYCSRLTIPFPFVIFAYIFMVMRKCFKCCCKKESKEPSVCCSRNEDNEILAWEA     1079
Great_tit_TRPM8      RFFLVQEYCSRLTIPFPFVIFAYIFMVMRKCFKCCCNKESKEPSICCSRNEDNEILAWEA     1063
                     *:*******.**.*****::***::**::*******:::. * . ** :***** *:**.
```

Fig. S13. Sequence alignment at the transmembrane domain among TRPM8 orthologs.

Residues covering the transmembrane helices S1 to S6 and the TRP domain are shown. Secondary structures based on the O and D states of mouse TRPM8 ($TRPM8_{MM}$) structures are indicated by rectangles and colored as in **fig. S1**. Sequence alignment was generated by the Clustal Omega program. Residue conservation is annotated by asterisks (*) for full conservation, colons (:) for strong similarity, and dots (.) for weak similarity. Residues involved in TC-I/AMG binding at the intersubunit interface above the S4-S5 linker are colored in green, while those for AMTB binding in the VSLD cavity in blue.

Sequence accession numbers – human TRPM8: UniProt Q7Z2W7; mouse TRPM8 ($TRPM8_{MM}$): UniProt Q8R4D5; rat TRPM8: UniProt Q8R455; chicken TRPM8: NCBI NP_001007083.2; collared flycatcher TRPM8 ($TRPM8_{FA}$): UniProt U3JD03; great tit TRPM8 ($TRPM8_{PM}$): NCBI XP_015489531.1.

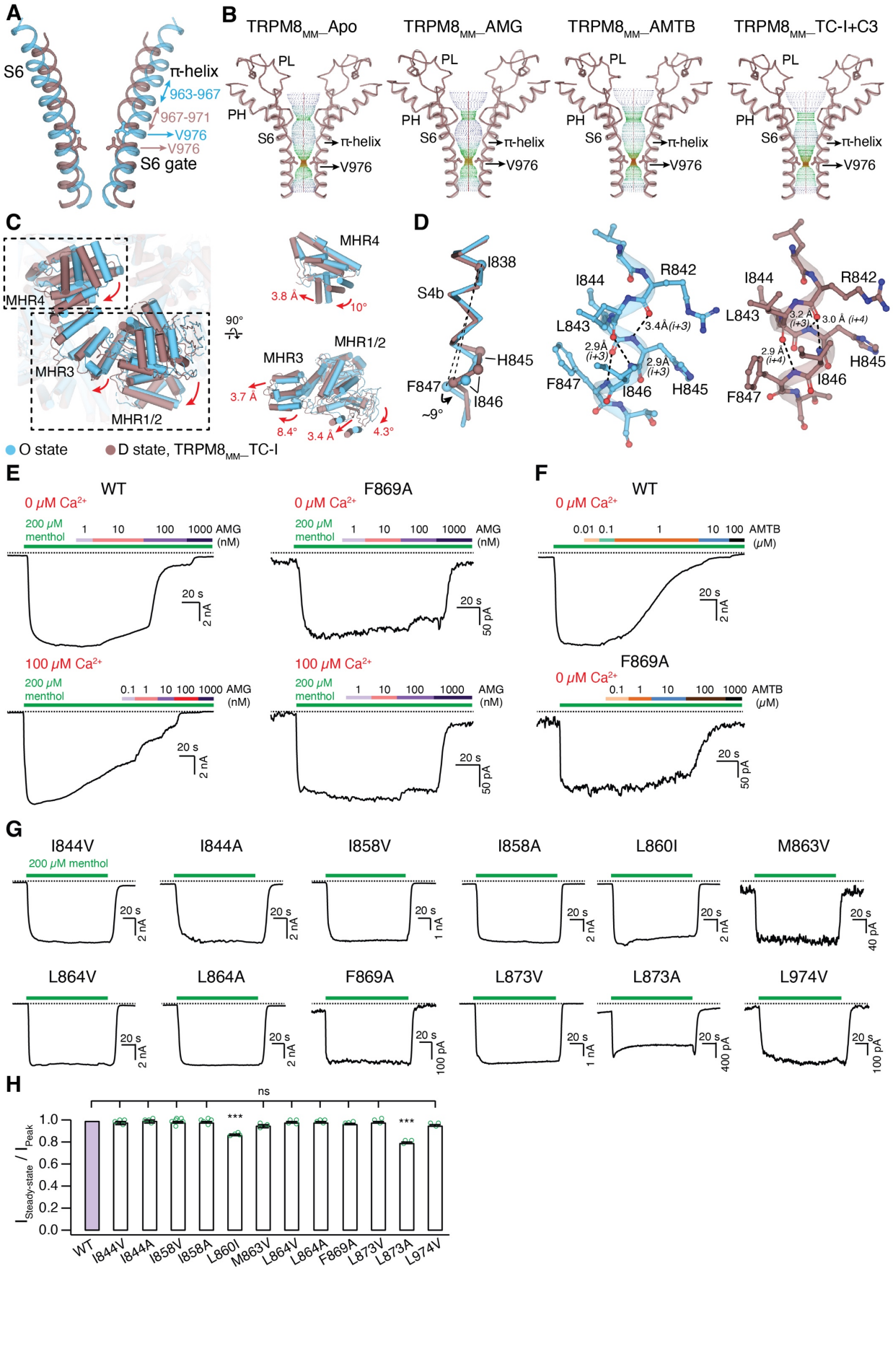
A
S6
π-helix
963-967
967-971
V976
V976
S6 gate
B
TRPM8MM_Apo
TRPM8MM_AMG
TRPM8MM_AMTB
TRPM8MM_TC-I+C3
PL
PH
S6
π-helix
V976
C
MHR4
MHR3
MHR1/2
3.8 Å
10°
90°
3.7 Å
8.4°
3.4 Å
4.3°
O state
D state, TRPM8MM_TC-I
D
I838
S4b
H845
F847
I846
~9°
I844
R842
L843
3.4Å(i+3)
2.9Å (i+3)
2.9Å (i+3)
3.2 Å (i+3)
3.0 Å (i+4)
2.9 Å (i+4)
E
WT
F869A
0 μM Ca2+
200 μM menthol
1 10 100 1000 AMG (nM)
20 s
2 nA
50 pA
100 μM Ca2+
0.1 1 10 100 1000 AMG (nM)
F
0.01 0.1 1 10 100 AMTB (μM)
G
I844V
I844A
I858V
I858A
L860I
M863V
L864V
L864A
F869A
L873V
L873A
L974V
1 nA
40 pA
400 pA
100 pA
H
ns
***
ISteady-state / IPeak
1.0
0.8
0.6
0.4
0.2
0.0
WT
I844V
I844A
I858V
I858A
L860I
M863V
L864V
L864A
F869A
L873V
L873A
L974V

Fig. S14. Mechanisms of TRPM8 desensitization and inhibition.

(**A**) Close-up comparison of S6 movement from O (blue) to D (brown) state, showing position changes in the S6 gate (Val^{976} in sticks) and the π-helix (two-headed arrows).

(**B**) Ion permeation pathway calculated from the HOLE diagram. The positions for the S6 gate residue and π-helix are denoted.

(**C**) Overlay (left) of the cytoplasmic MHR1 to 4 domains between the O state (blue) and the D state $TRPM8_{MM}$_TC-I (brown). Insets (right) showing close-up views at the dashed boxes from the left panel. Channel structures shown as cartoon cylinders. Red arrows indicate movements from O to D state with distances and angles denoted.

(**D**) Superimposed (left) and side-by-side (middle and right) comparison of the S4b helical configuration between the O (blue) and the D (brown) states. Arrows indicate rearrangement in S4b. Dashed lines indicate the hydrogen bonds in the helical backbones.

(**E**) Representative currents of the WT (left) and $Phe^{869}Ala$ (right) $TRPM8_{MM}$ channels at –60 mV in HEK293T cells. Current traces elicited by 200 μM menthol was inhibited by increasing concentrations of AMG in the presence of 0 μM (top) and 100 μM (bottom) extracellular Ca^{2+}.

(**F**) Representative currents of the WT (top) and $Phe^{869}Ala$ (bottom) $TRPM8_{MM}$ channels at –60 mV in HEK293T cells. Current traces elicited by 200 μM menthol was inhibited by increasing concentrations of AMTB.

(**G**) Representative currents of the mutant $TRPM8_{MM}$ channels at –60 mV in HEK293T cells. Current traces elicited by 200 μM menthol for 2 min.

(**H**) Summary of currents remained after desensitization for the WT and mutant $TRPM8_{MM}$ channels activated by menthol (n = 3–6). Summary data of the WT (purple bar) from **Fig. 4K** is reproduced to facilitate visual comparison. Open circles indicate the individual data points for each experiment. ns > 0.05, ***P < 0.001, using one-way ANOVA followed by Dunnett post-hoc test. Data are mean ± SEM.

Dotted lines in **E** to **G** indicate the zero-current level.

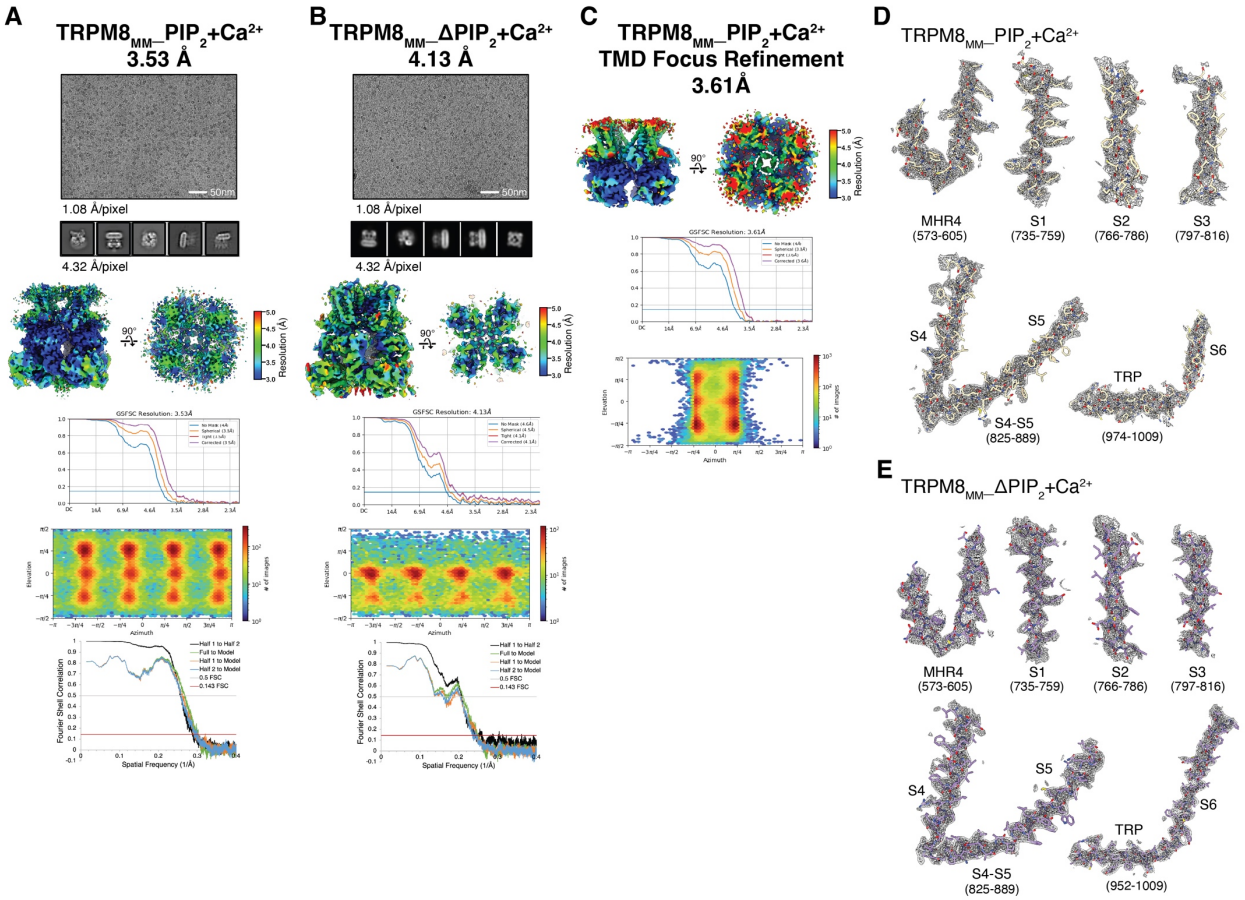

Fig. S15. Cryo-EM data collection and validation, part III.

(**A** and **B**) Representative micrographs, 2D classification images, local resolution estimation, the Fourier shell correlation (FSC) curves of the final 3D reconstruction with different masking calculated in CryoSPARC, orientation distribution diagram, and the FSC curves between model and full- or half-maps calculated in PHENIX. Results are shown for TRPM8$_{MM}$_PIP$_2$+Ca^{2+} (**A**) and TRPM8$_{MM}$_ΔPIP$_2$+Ca^{2+} (**B**), respectively. The pixel sizes are specified below the images.

(**C**) Local resolution estimation, the Fourier shell correlation (FSC) curves of the final 3D reconstruction with different masking calculated in CryoSPARC, and orientation distribution diagram for the TMD focused refinement on TRPM8$_{MM}$_PIP$_2$+Ca^{2+}.

(**D** and **E**) Representative EM densities (gray mesh) for key structural elements in TRPM8$_{MM}$_PIP$_2$+Ca^{2+} (**D**), TRPM8$_{MM}$_ΔPIP$_2$+Ca^{2+} (**E**). Thresholding at 0.15 in (**D**), 0.18 or 0.2 in (**E**).

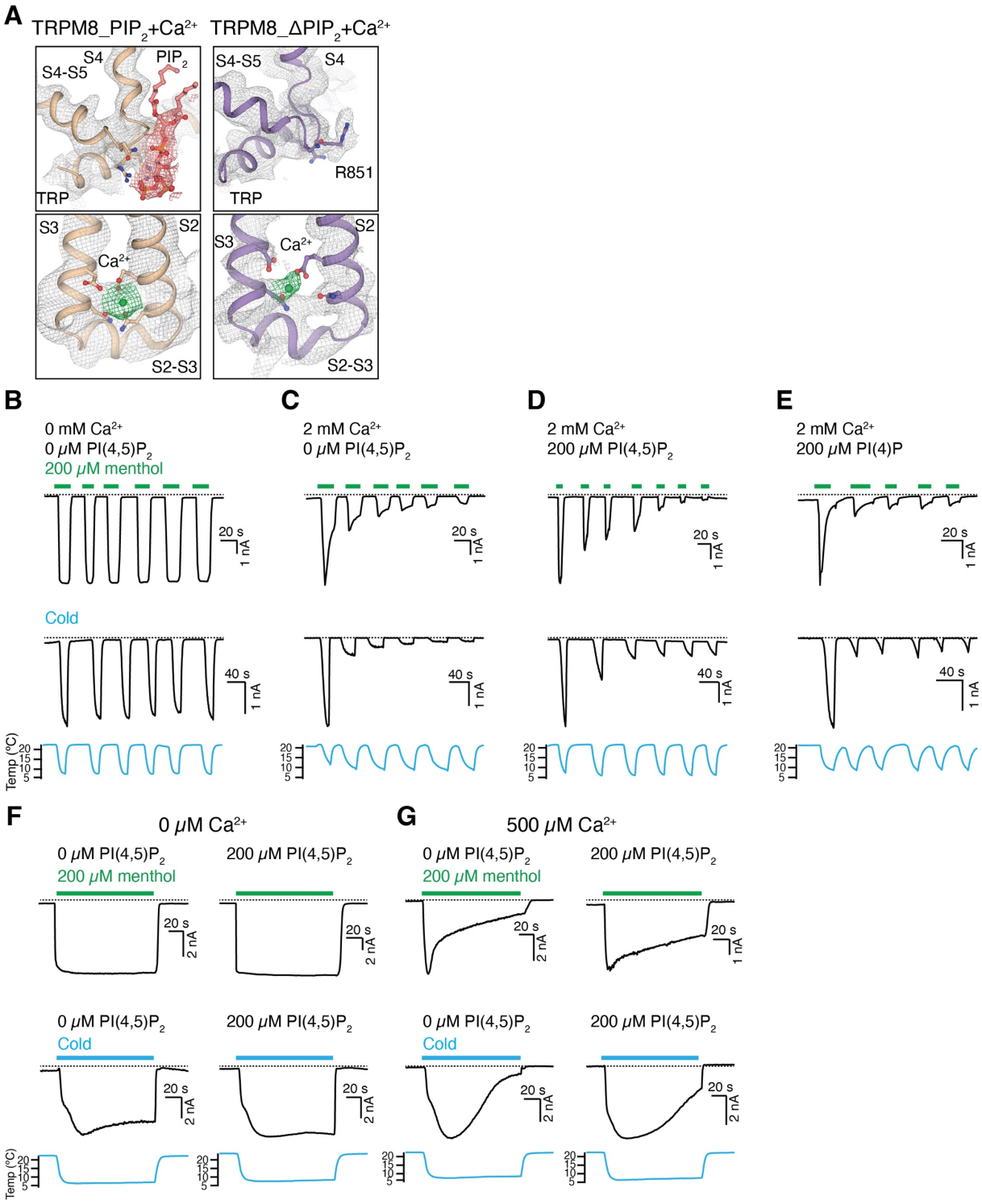

Fig. S16. The roles of PIP_2 and Ca^{2+} in TRPM8 desensitization.

(**A**) EM densities at the interfacial cavity (top) and the VSLD cavity (bottom) in $TRPM8_{MM}$_PIP_2+Ca^{2+} (left, wheat) and $TRPM8_{MM}$_ΔPIP_2+Ca^{2+} (right, purple) structures. Densities are contoured at 0.15 and 0.2 for channel (gray mesh), 0.13 for PIP_2 (red mesh), 0.14 for Ca^{2+} (green mesh) in $TRPM8_{MM}$_PIP_2+Ca^{2+}, and contoured at 0.19 and 0.2 for channel (gray mesh) and 0.2 for Ca^{2+} (green mesh) in $TRPM8_{MM}$_ΔPIP_2+Ca^{2+}.

(**B** to **E**) Representative time courses of $TRPM8_{MM}$ activation at –60 mV in HEK293T cells. Current traces elicited by 200 μM menthol (top) or cold (bottom) in the presence of 0 mM extracellular Ca^{2+} and 0 μM diC8-PI(4,5)P_2 in the intracellular pipette solution (**B**), 2 mM extracellular Ca^{2+} and 0 μM diC8-PI(4,5)P_2 in the intracellular pipette solution (**C**), 2 mM extracellular Ca^{2+} and 200 μM diC8-PI(4,5)P_2 in the intracellular pipette solution (**D**), 2 mM extracellular Ca^{2+} and 200 μM diC8-PI(4)P in the intracellular pipette solution (**E**).

(**F** and **G**) Representative currents of the WT $TRPM8_{MM}$ channels at –60 mV in HEK293T cells. Current trace elicited by 200 μM menthol (top) or cold (bottom) for 2 min in the presence of 0 μM (**F**) or 500 μM (**G**) extracellular Ca^{2+}. Currents were recorded without (left) or with (right) 200 μM diC8-PI(4,5)P_2 in the intracellular pipette solution.

Dotted lines in **B** to **G** indicate the zero-current level.

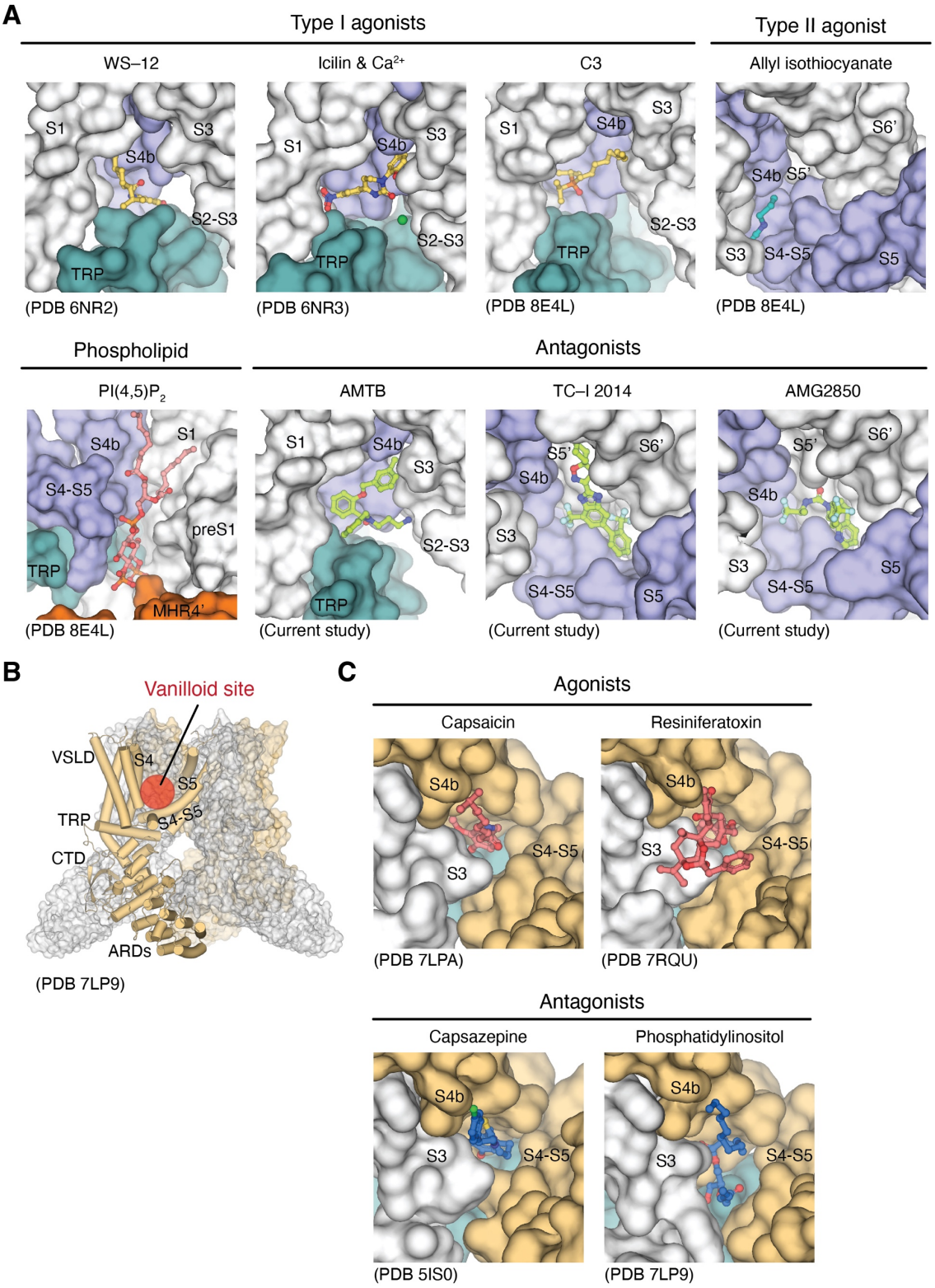

Fig. S17. Comparison of ligand binding to TRPM8 and TRPV1 channels.

(**A**) Binding sites for type I agonists (WS-12, icilin, C3), type II agonists (AITC), PI(4,5)P_2, and antagonists (AMTB, TC-I, AMG) in TRPM8 channels.

(**B**) Architecture of TRPV1 channels and the vanilloid binding site.

(**C**) Binding sites for agonists (capsaicin, resiniferatoxin) and antagonists (capsazepine, phosphatidylinositol) in TRPV1 channels.

Ligand binding sites are shown in surfaces and ligand molecules in sticks. PDB IDs are specified.

Table S1. Cryo-EM data collection, refinement, and validation statistics.

	$TRPM8_{MM}$ _PIP_2+Ca^{2+} (PDB-9B6J, EMD-44261) **Full map**	**$TRPM8_{MM}$ _ΔPIP_2+Ca^{2+}** (PDB-9B6K, EMD-44262) **Full map**	**$TRPM8_{MM}$ _apo D state** (PDB-9B6D, EMD-44255) **Full map**	**$TRPM8_{MM}$ _TC-I** (PDB-9B6E, EMD-44256) **Full map**
Data collection and Processing				
Microscope	Titan Krios	Titan Krios	Titan Krios	Titan Krios
Voltage (keV)	300	300	300	300
Camera	K3	K3	K3	K3
Nominal magnification*	81,000×	81,000×	81,000×	81,000×
Physical pixel size (Å $pixel^{-1}$)*	1.08	1.08	1.1	1.08
Total electron exposure (e^- $Å^{-2}$)	60	60	53	60
Exposure rate (e^- $pixel^{-1}$ s^{-1})	15	15	17	30
Number of frames	60	60	53	40
Defocus range (μm)	-0.7 to -2.2	-0.7 to -2.2	-0.7 to -2.5	-0.7 to -2.2
Automation software	Latitude	Latitude	EPU	Latitude
Energy filter slit width (eV)	20	20	20	20
Micrographs collected (no.)	10,045	9,400	10,568	9,581
Micrographs used (no.)	9,261	9,381	8,844	9,471
Total extracted particles (no.)	3,143,850	3,345,503	2,405,897	2,896,859
Reconstruction				
Refined particles (no.)	1,371,900	1,974,786	1,415,860	1,601,803
Final particles (no.)	103,487	35,327	87,176	194,290
Symmetry imposed	C4	C4	C4	C4
Resolution (global, Å)	3.53 Å	4.13 Å	3.30 Å	2.91 Å
FSC 0.5 (unmasked/masked)	4.5 / 3.9 Å	7.4 / 4.2 Å	4.1 / 3.6 Å	3.7 / 3.3 Å
FSC 0.143 (unmasked/masked)	4.0 / 3.5 Å	4.2 / 3.6 Å	3.7 / 3.3 Å	3.3 / 2.9 Å
Map sharpening B-factor ($Å^2$)	-60	-139	-75	-40
Map sharpening methods	global sharpening	global sharpening	global sharpening	global sharpening
Model composition				
Protein residues	3584	3676	3732	3720
Ligand	4	0	20	20
Ion	4	4	0	0
Model refinement				
Refinement package	Coot, PHENIX	Coot, PHENIX	Coot, PHENIX	Coot, PHENIX
Map Correlation Coefficient	0.71	0.68	0.80	0.76
B factors ($Å^2$)				
Protein residues	164.83	147.85	92.78	120.65
Ligands	178.70	124.95	51.26	85.68
R.m.s. deviations				
Bond lengths (Å)	0.004	0.002	0.003	0.003
Bond angles (°)	0.703	0.461	0.686	0.753
Validation				
MolProbity score	1.65	1.72	1.51	1.62
Clashscore (all atoms)	11.87	8.05	5.16	5.6
Poor rotamers (%)	0.00 %	0.96 %	0.30 %	0.00 %
Ramachandran				
Outliers	0.00 %	0.00 %	0.00 %	0.00 %
Allowed	2.29 %	4.12 %	3.53 %	4.61 %
Favored	97.71 %	95.88 %	96.47 %	95.39 %

	$TRPM8_{MM}$ _AMG (PDB-9B6F, EMD-44257) **Full map**	**$TRPM8_{MM}$ _AMTB** (PDB-9B6G, EMD-44258) **Full map**	**$TRPM8_{MM}$ _TC-I+C3** (PDB-9B6H, EMD-44259) **Full map**	**$TRPM8_{PM}$ _TC-I** (PDB-9B6I, EMD-44260) **Full map**
Data collection and Processing				
Microscope	Titan Krios	Titan Krios	Titan Krios	Titan Krios
Voltage (keV)	300	300	300	300
Camera	K3	K3	K3	K3
Nominal magnification*	81,000×	81,000×	81,000×	81,000×
Physical pixel size (Å $pixel^{-1}$)*	1.1	1.08	1.08	1.08
Total electron exposure (e^- $Å^{-2}$)	53	60	60	60
Exposure rate (e^- $pixel^{-1}$ s^{-1})	17	30	30	30
Number of frames	53	40	40	40
Defocus range (μm)	-0.7 to -2.5	-0.7 to -2.2	-0.7 to -2.2	-0.7 to -2.2
Automation software	EPU	Latitude	Latitude	Latitude
Energy filter slit width (eV)	20	20	20	20
Micrographs collected (no.)	9,395	10,053	14,226	10,266
Micrographs used (no.)	8,793	9,798	14,059	9717
Total extracted particles (no.)	2,608,765	3,194,454	4,913,002	3,535,129
Reconstruction				
Refined particles (no.)	1,220,108	1,517,018	2,031,558	1,567,180
Final particles (no.)	84,589	67,871	112,062	82,123
Symmetry imposed	C4	C4	C4	C4
Resolution (global, Å)	3.42 Å	2.81 Å	2.76 Å	3.26 Å
FSC 0.5 (unmasked/masked)	4.2 / 3.8 Å	3.9 / 3.3 Å	3.9 / 3.3 Å	4.1 / 3.6 Å
FSC 0.143 (unmasked/masked)	3.8 / 3.4 Å	3.3 / 2.8 Å	3.3 / 2.8 Å	3.6 / 3.3 Å
Map sharpening B-factor ($Å^2$)	-75	-50	-30	-60
Map sharpening methods	global sharpening	global sharpening	global sharpening	global sharpening
Model composition				
Protein residues	3716	3664	3736	3424
Ligand	20	28	24	20
Ion	0	0	0	4
Model refinement				
Refinement package	Coot, PHENIX	Coot, PHENIX	Coot, PHENIX	Coot, PHENIX
Map Correlation Coefficient	0.81	0.73	0.76	0.81
B factors ($Å^2$)				
Protein residues	112.20	128.13	118.52	78.70
Ligands	58.39	93.97	99.87	32.82
R.m.s. deviations				
Bond lengths (Å)	0.003	0.003	0.004	0.003
Bond angles (°)	0.703	0.704	0.706	0.698
Validation				
MolProbity score	1.50	1.42	1.61	1.40
Clashscore (all atoms)	5.1	5.4	7.51	5.42
Poor rotamers (%)	0.31 %	0.00 %	0.44 %	0.27 %
Ramachandran				
Outliers	0.00 %	0.00 %	0.00 %	0.00 %
Allowed	3.52 %	2.68 %	3.17 %	2.52 %
Favored	96.48 %	97.32 %	96.83 %	97.48 %

*Calibrated pixel size at the detector